Keck Planet Finder: preliminary design

Steven R. Gibson, Andrew W. Howard, Arpita Roy, Christopher Smith, Sam Halverson, et al.

Steven R. Gibson, Andrew W. Howard, Arpita Roy, Christopher Smith, Sam Halverson, Jerry Edelstein, Marc Kassis, Edward H. Wishnow, Michael Raffanti, Steve Allen, Jason Chin, David Coutts, David Cowley, Jim Curtis, William Deich, Tobias Feger, Daniel Finstad, Yulia Gurevich, Yuzo Ishikawa, Ean James, Elisha Jhoti, Kyle Lanclos, Scott Lilley, Tim Miller, Steve Milner, Tom Payne, Kodi Rider, Constance Rockosi, Dale Sandford, Christian Schwab, Andreas Seifahrt, Martin M. Sirk, Roger Smith, Julian Stuermer, Marie Weisfeiler, Mavourneen Wilcox, Adam Vandenberg, Peter Wizinowich, "Keck Planet Finder: preliminary design," Proc. SPIE 10702, Ground-based and Airborne Instrumentation for Astronomy VII, 107025X (6 July 2018); doi: 10.1117/12.2311565

Event: SPIE Astronomical Telescopes + Instrumentation, 2018, Austin, Texas, United States

Keck Planet Finder: Preliminary Design

Steven R. Gibson[a], Andrew W. Howard[b,a], Arpita Roy[b], Christopher Smith[a], Sam Halverson[c,d,*], Jerry Edelstein[a], Marc Kassis[e], Edward H. Wishnow[a], Mike Raffanti[a], Steve Allen[f], Jason Chin[e], David Coutts[h], David Cowley[f], Jim Curtis[a], William Deich[f], Tobias Feger[h], Daniel Finstad[a,n], Yulia Gurevich[k], Yuzo Ishikawa[a,m], Ean James[e], Elisha Jhoti[a,j], Kyle Lanclos[e], Scott Lilley[e], Tim Miller[a], Steve Milner[e], Tom Payne[a,l], Kodi Rider[a], Constance Rockosi[f,g], Dale Sandford[f], Christian Schwab[h], Andreas Seifahrt[i], Martin M. Sirk[a], Roger Smith[b], Julian Stuermer[i], Marie Weisfeiler[a], Mavourneen Wilcox[e], Adam Vandenberg[e], and Peter Wizinowich[e]

[a]Space Sciences Laboratory, University of California, Berkeley, United States
[b]California Institute of Technology, Pasadena, United States
[c]University of Pennsylvania, Philadelphia, United States
[d]Massachusetts Institute of Technology, Cambridge, United States
[e]W. M. Keck Observatory, Kamuela, United States
[f]University of California Observatories, Santa Cruz, United States
[g]University of California, Santa Cruz, United States
[h]Macquarie University, Sydney, Australia
[i]University of Chicago, Chicago, United States
[j]University of Edinburgh, Edinburgh, UK
[k]Heidelberg University, Heidelberg, Germany
[l]University of Manchester, Manchester, UK
[m]San Francisco State University, San Francisco
[n]Syracuse University, Syracuse, United States
[*]NASA Sagan Fellow

ABSTRACT

The Keck Planet Finder (KPF) is a fiber-fed, high-resolution, high-stability spectrometer in development for the W.M. Keck Observatory. The instrument recently passed its preliminary design review and is currently in the detailed design phase. KPF is designed to characterize exoplanets using Doppler spectroscopy with a single measurement precision of $0.5\,\mathrm{m\,s^{-1}}$ or better; however, its resolution and stability will enable a wide variety of other astrophysical pursuits. KPF will have a 200 mm collimated beam diameter and a resolving power greater than 80,000. The design includes a green channel (445 nm to 600 nm) and red channel (600 nm to 870 nm). A novel design aspect of KPF is the use of a Zerodur optical bench, and Zerodur optics with integral mounts, to provide stability against thermal expansion and contraction effects.

Keywords: Spectrometer, exoplanets, Doppler spectroscopy, radial velocity, Zerodur

1. INTRODUCTION

The Keck Planet Finder (KPF) is a fiber-fed, high-resolution, high-stability spectrometer in development for the W.M. Keck Observatory (WMKO). The instrument is designed to characterize exoplanets via Doppler spectroscopy with a single measurement precision of $0.5\,\mathrm{m\,s^{-1}}$ or better; however, its resolution and stability will enable a wide variety of other astrophysical pursuits. KPF will cover a wavelength range of 445 nm to 870 nm

Corresponding author email: sgibson@ssl.berkeley.edu

Ground-based and Airborne Instrumentation for Astronomy VII, edited by Christopher J. Evans, Luc Simard, Hideki Takami,
Proc. of SPIE Vol. 10702, 107025X · © 2018 SPIE · CCC code: 0277-786X/18/$18 · doi: 10.1117/12.2311565

over green and red channels. The project is now in the detailed design phase, having passed the Preliminary Design Review (PDR) in November 2017. First light is expected in late 2020.

Several institutions contribute to the KPF project: the Space Sciences Laboratory (SSL) at UC Berkeley is the primary design and build location; WMKO is responsible for the fiber injection unit (FIU), facility modifications, and instrument software; University of California Observatories (UCO) is working on the detectors and the instrument software; the California Institute of Technology (Caltech) is developing the data reduction pipeline and is also involved with the design and testing of the detectors; and Macquarie University is developing the Fabry-Pérot etalon for the KPF calibration system.

2. SCIENCE CASE

KPF will be a broadly capable high-resolution optical spectrometer. Its primary science driver is to measure the masses and orbital properties of Earths, super-Earths, and sub-Neptunes that are known to be common from Doppler surveys[1–3] and the Kepler mission.[4] To do this, KPF will measure precise stellar Doppler shifts due to the gravitational pull of orbiting planets and allow inference of planetary properties. KPF will be used to discover planets, particularly around nearby, bright stars and will excel at measuring the masses of planets discovered by transiting programs such as Kepler, TESS, and PLATO.

KPF will be particularly effective for transiting planet follow-up because of the Doppler precision (requirement: 0.5 $\mathrm{m\,s^{-1}}$ systematic error floor; goal: 0.3 $\mathrm{m\,s^{-1}}$) and the collecting area of the 10 m Keck telescope. Two primary requirements drive the KPF design: minimizing errors in Doppler shifts caused by instrumental effects, and maximizing optical throughput. In the expected discovery space for TESS (Figure 1), KPF will measure planet masses for stars as faint as $V \approx 15$ mag, while similar precision instruments on 3 m class instruments will struggle to reach fainter than magnitude 12.5. Thus, KPF will be able to measure the masses of hundreds of TESS-discovered planets to map out the diversity of planet masses and densities (a clue to composition) in the Earth-to-Neptune regime. KPF will also be able to measure the mass function of Earth-size planets from Kepler to determine if such planets are commonly rocky or are enveloped in thick, low-density envelopes.

For nearby stars, KPF will catalog the planets in the solar neighborhood and will provide targets for planet imaging by WFIRST and giant segmented mirror telescopes (GSMTs; 30 m class). Planets orbiting early M dwarfs are particularly compelling because Earth-mass planets in the traditionally-defined Habitable Zone are detectable with KPF and these planets are also imageable by GSMTs.

Additional science cases for KPF stem from its general use as a high-resolution optical spectrometer and its high stability. These include stellar characterization, exoplanet atmosphere spectroscopy, detection of the expansion of the universe in real time with Lyman-α forest spectroscopy, galactic chemical abundance archaeology, spectroscopy of solar system objects, and isotopic abundance measurements from precise line shapes.

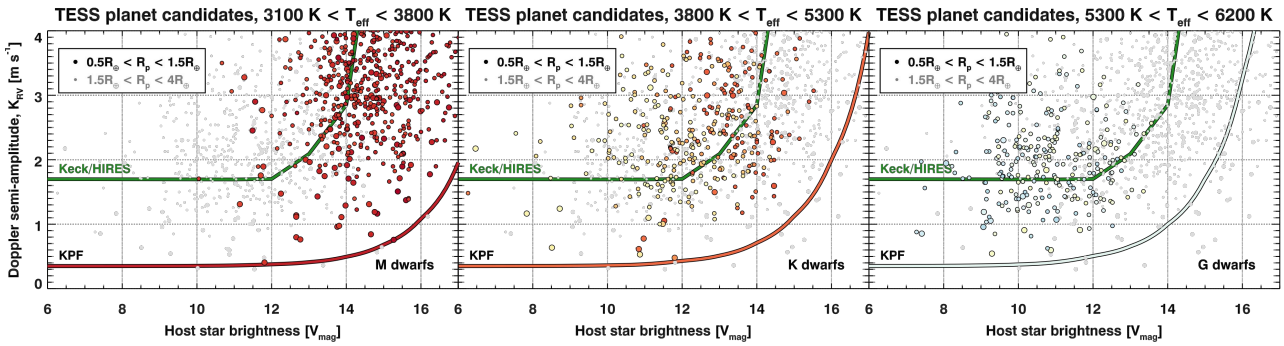

Figure 1. Expected planet discovery space for NASA's TESS mission with estimated sensitivity curves for KPF (Red/Orange/blue colored lines) and HIRES (green) at Keck Observatory. Planet-hosting stars are separated into spectral type bins, ranging from cooler M-dwarfs (left) to warmer Sun-like stars (middle, right). Super-Earth planets (R_p = 1.5–4 $R_\oplus$) are denoted by smaller points, while Earth-size planets (R_p = 0.75–1.5 $R_\oplus$) are shown as larger points. The planet sample is from a simulation of the TESS mission survey yield.[5] Point colors trace effective temperature of the host star.

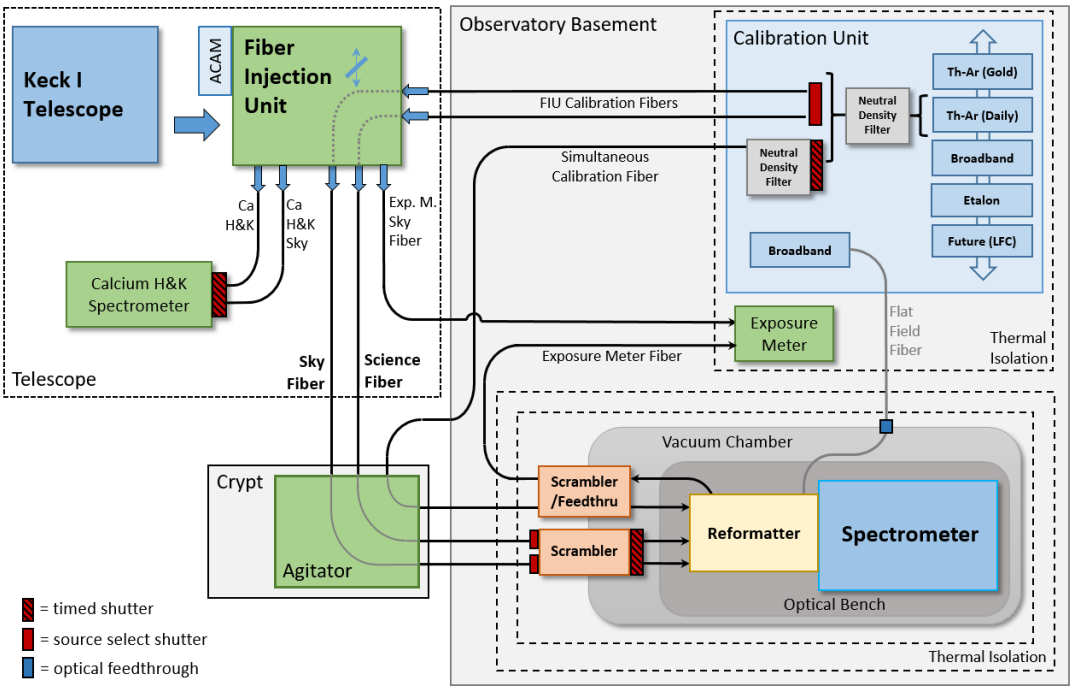

Figure 2. Schematic overview of the KPF system. The fiber injection unit will utilize the existing acquisition cam (ACAM) on the adaptive optics system bench. The spectrometer, calibration unit and exposure meter will be located within the observatory basement. The fiber agitator (for modal noise suppression) will be located in the "crypt", which is a small room directly underneath the azimuth axis of the telescope, connecting the dome and the coudé tunnel to the observatory basement. The Calcium H & K spectrometer will be located on the telescope with the fiber injection unit.

3. SYSTEM OVERVIEW

The KPF instrument will be comprised of several subsystems, each of which is described within this section. An overview schematic of the KPF system is shown in Figure 2.

3.1 Notable design changes during the preliminary design phase

For reference, major design changes since the 2016 KPF SPIE paper[6] are listed here.

- **Telescope:** KPF will now use Keck I, instead of Keck II. This choice was made considering the current and future relative demand between the telescopes. Also, for intra-night instrument changes, Keck I is favored since rapid instrument switching with the Deployable Tertiary Mirror (K1DM3[7]) will enable scheduling KPF for short intervals of time. This approach facilitates high-cadence observations that we expect will be needed for the lowest-amplitude Doppler signals, particularly when stellar activity signals must be disentangled.

- **FIU Location:** The fiber injection unit has moved from an instrument cart to the Keck I adaptive optics (AO) bench. It will be located on an unused section of the the AO bench but does not utilize the AO system for observations. This was a desirable change for several reasons: the FIU is now protected within a clean room; the FIU does not need to move when KPF goes on-sky (only a small fold mirror translates into the beam from the telescope); the Calcium H & K spectrometer can be placed in the same room as the FIU, which allows for a major reduction in fiber length between the FIU and that auxiliary spectrometer; and KPF can utilize the existing AO bench target acquisition system.

- **Spectrometer Location:** The KPF spectrometer will now be placed at the Keck I end of the observatory basement hallway. This decision was the result of a major trade study and measurement campaign to determine the most stable location at the observatory for the spectrometer. Two primary locations

were considered: the basement hallway and the Keck I dome floor. For each location, factors explored included fiber length, ease and safety of access, temperature stability, the vibration environment, operational/maintenance costs and concerns, and facility modifications required. While it was a close trade between the two locations, in the end temperature stability was the primary driver for the basement hallway location, albeit at a cost of ease of access.

- **Opto-mechanics:** The optical elements will interface with the Zerodur bench through Zerodur shims. The earlier design had the optics and mounts directly contacting the Zerodur bench. Including shims at this interface allows for a fine-tuning of the position of each optic to account for fabrication tolerances. More details are provided below in Section 4.1.

- **Exposure Meter:** A photometer-based design has been replaced with a spectrometer to provide chromatic information. See Section 3.11 for details.

- **Calcium H & K Spectrometer:** This spectrometer now employs an echelle grating as the primary disperser. Details are given below in Section 3.10.

- **Calibration Sources:** A thorium-argon hollow cathode lamp is no longer the only calibration source for tracking the instrument zero-point: a Fabry-Pérot etalon will provide a high line-density calibration source (see Section 3.9 below for details).

- **Science Fiber:** A refined analysis and trade study changed the science fiber size from 250 μm to 225 μm. Factors considered included the average seeing conditions, percentage of nights on either side of the median seeing value, fiber injection parameters (f/number, plate scale at fiber), number of slices within the reformatter, and spectral format considerations.

- **Vacuum Chamber:** The broad, flat surfaces on the previously shown vacuum chamber[6] have proven difficult to sufficiently brace with welded ribs. As such, we have moved to a more traditional vacuum chamber design as shown in Section 4.2. The whiffletree bench support within the chamber has also been replaced by separate vacuum-compatible isolators. This approach moves the isolators closer to the bench (offering higher stability), and also avoids the CTE mismatch that was present between the whiffletree's metal components and the Zerodur bench.

3.2 Fiber Injection Unit

Light from the Keck I telescope will feed the KPF fiber injection unit, which will be located on the adaptive optics optical bench on the left Nasmyth platform of the Keck I telescope. The optical layout is shown in Figure 3. The FIU will include an atmospheric dispersion corrector (ADC), a tip/tilt mirror system for image stabilization, and a calibration light input (a fold mirror will translate into and out of the beam as required). For acquiring targets, KPF will utilize the existing AO system acquisition camera. The FIU also focuses light from the telescope onto a science fiber and two sky fibers (to monitor contamination from moonlight and the sky background), and two fibers sending ultraviolet (UV) light to the Calcium H & K spectrometer. Within the Calcium H & K arm is a fused silica prism, with the prism angle optimized to minimize atmospheric dispersion at a zenith angle of 40 degrees (the mid-point of our observing elevation range).

The design, assembly and testing the FIU will be the responsibility of WMKO. This is an ideal arrangement, as the FIU will directly interface with the telescope itself and also with its guiding and control software.

3.3 Illumination Homogenization System

Stable illumination of the spectrometer is paramount as any changes of the light distribution in either the image or pupil planes can cause displacements of the spectrum that closely mimic Doppler shifts. An optical fiber feed is well known to serve as a "scrambler", suppressing illumination changes at the input to the fiber (at the telescope focal plane) to produce a more homogeneous output at the spectrometer.[8] To improve the scrambling performance, the science fiber will be an octagonal fiber,[9,10] and the fiber system will include additional scrambling,[11] consisting of a pair of doublet lenses,[12] that swap the near and far fields of the fiber output. The

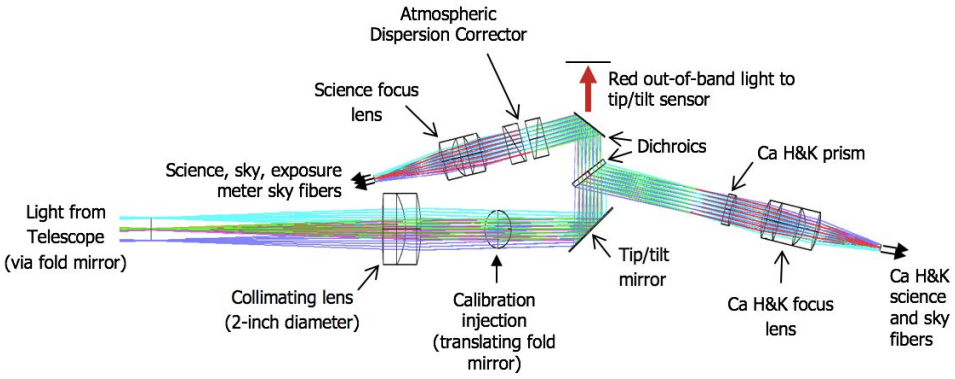

Figure 3. Optical layout of the fiber injection unit.

scrambler then feeds a short, 5 m length of octagonal fiber to further homogenize the scrambler output. In the KPF scrambler design, a vacuum window is placed between the lenses, allowing the scrambler system to double as a vacuum feedthrough.

Fiber modal noise can also cause illumination instabilities at the output of a fiber,[13,14] and limit the achievable signal-to-noise ratio, especially in a sliced beam.[15] To mitigate this effect, KPF employs a mechanical agitator (of a design based on the HPF agitator[16]) that will impose a periodic perturbation on all three (science, sky, and simultaneous calibration) fibers. We note here that the light path is made as similar as possible for all three fibers in order to maintain maximum fidelity between their outputs.

Prototypes of the KPF scrambler and agitator systems have been built and tested in our laboratory. Full details on the designs of these subsystems, as well as test results, are presented within Sirk et al. (2018).[17]

3.4 Optical Fibers

Fifteen individual optical fibers are utilized within the KPF system, as shown in Figure 2. We have adopted a scheme of having separate fibers outside and inside of the vacuum chamber, with two dual-path scrambler systems allowing the light from the primary fibers to pass through the vacuum chamber wall (the infrequently-used alternative flat field fiber that overfills the beam traces will utilize an off-the-shelf optical vacuum feedthrough). This approach has several advantages: one can replace the external fibers (if damaged) without opening the vacuum chamber; the alignment of the fibers with respect to the spectrometer is protected within the vacuum chamber (and therefore less likely to be disturbed); and the fibers are not bonded within a vacuum feedthrough which can increase focal ratio degradation (FRD). As such, while there are fifteen individual fibers, there are only ten discrete fiber paths within the KPF system.

A key driver for the science fiber is to keep its length as short as possible, as the system efficiency at the blue end of the green channel is especially affected by the internal transmission of this fiber. WMKO has determined the shortest fiber path possible from the FIU on the Nasmyth platform to the spectrometer in the basement (Figure 4). The 60-m long science and sky fibers will follow this path, which negotiates the telescope structure and then follows the coudé tunnel to the main spectrometer within the observatory basement. To accommodate telescope movements, near the center point of this path sits a fiber wrap that is coaxial with the azimuth rotation axis of the telescope. A custom fiber wrap for KPF was designed by WMKO, which only requires 1.2 m of fiber (compared to the approximately 22 m of fiber that the existing cable wrap on the telescope would have required).

3.5 Reformatter

Following the scrambler, the science fiber ends at the input to the reformatter. This system (Figure 5) takes the light leaving the science fiber, and rearranges it into three "slices", aligned along the spectrometer (virtual) slit. This system effectively allows the KPF spectrometer to be three times smaller than a traditional spectrometer would be, given the aperture and image scale of the Keck telescope. It allows a large fiber to be used at the

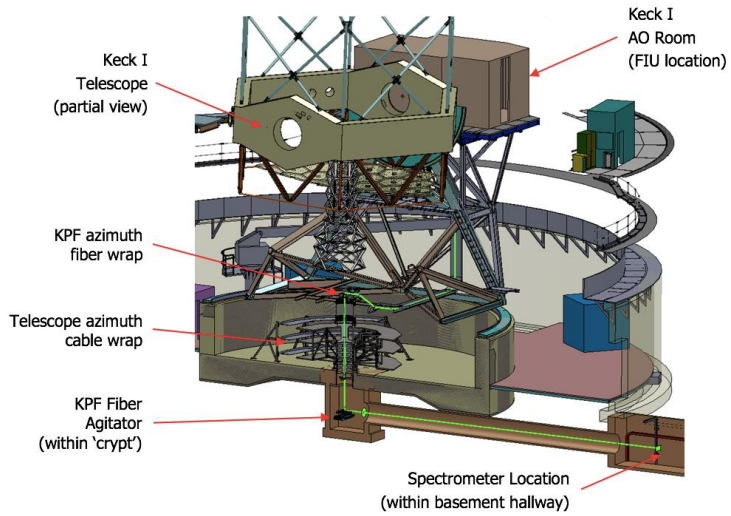

Figure 4. Fiber path (in green) from the Keck I AO room (FIU location) to the observatory basement (spectrometer location). The telescope azimuth cable wrap is indicated, but was avoided through the use of a significantly smaller KPF-specific fiber wrap.

telescope focal plane (for seeing-limited collection of starlight), while presenting the spectrometer with a narrow "slit width" (which allows high resolution).

Light from the science, sky, and simultaneous calibration fiber is incident on the reformatter, as shown at the left of Figure 5. A triplet lens magnifies the fiber outputs by a factor of ten, and forms an image of them on the image slicing mirrors. The science fiber image falls on three slicing mirrors, which then redirect the separate slices toward the pupil mirrors, which refocus the light to an intermediate image. The sky and simultaneous calibration fiber images are not sliced, but rather fall on separate mirrors on either side of the slicing and pupil mirrors, and also reach focus at the intermediate image. This intermediate image is then de-magnified by a pair of relay mirrors, to form an f/8 image at the slit position of the spectrometer. To maintain the same slit width across all slices and fibers, the mirrors at the image slicing location for the sky and simultaneous calibration fibers have the same width in the spectral direction as the science slicer mirrors (effectively applying a mask to the images of those fibers).

The optical design of the reformatter is based on that shown in Vivès et al. 2016.[18] Winlight Systems has undertaken two design studies on this system for KPF, during which they have optimized the design for our

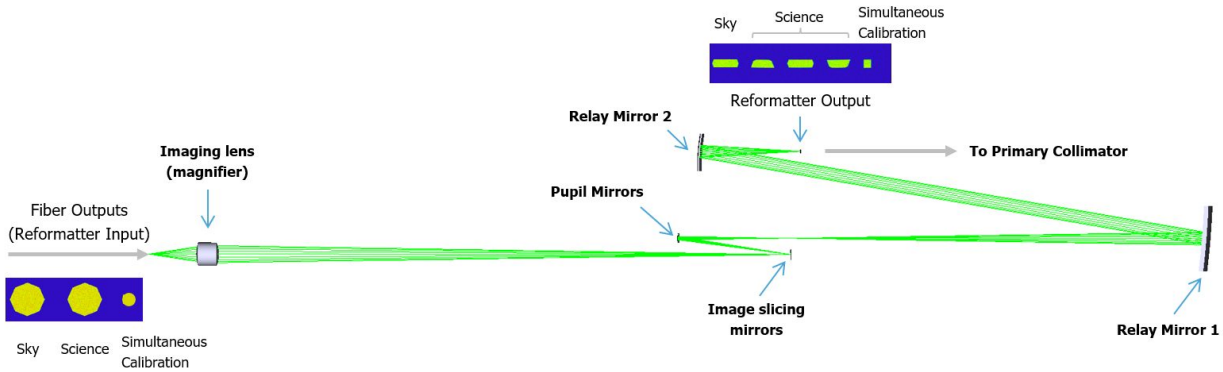

Figure 5. Optical design of the KPF reformatter. The inset at top right shows the image presented at the spectrometer slit location, with the science fiber sliced three times and the calibration and sky fiber outputs masked to have the same width in the spectral direction as the science slices. These five images are the sources for the five "orderlets" within each echelle order in KPF spectra.

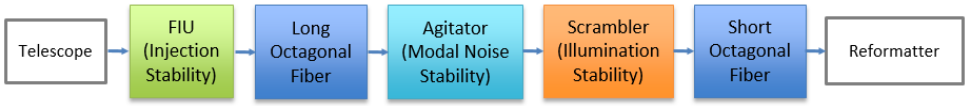

Figure 6. Components of the KPF illumination homogenization system.

requirements, and also toleranced it for manufacture. Going forward there will be one more detailed design study by Winlight Systems, after which they will fabricate the device, with the reformatter mirrors being optically contacted to a Zerodur base for high mechanical stability.[19]

An important point to note is that the reformatter is presented with a uniformly illuminated source to be sliced, as it is fed by the output of the entire illumination homogenization system (Figure 6). This is a very different situation than placing a traditional slicer at the focal plane of a telescope, where the illumination stability suffers from seeing and guiding issues. By placing the reformatter after the homogenization system, the intent is to minimize the changes in illumination between each slice. This is an important stability concern, and the illumination stability resulting from our our fiber, agitator, and scrambler system has been tested in the laboratory, with results presented in Sirk et al. (2018).[17]

We intend to treat each science slice independently during reduction. Due to alignment tolerances during the fabrication of the reformatter, we expect unavoidable offsets in the wavelength solution between slices, and therefore we will not simply collapse the three slices together, but rather treat each as an independent measurement during reduction.

3.6 Spectrometer Optical Design

The convergence of the precision radial velocity (PRV) community on white pupil spectrometers is evident by a survey of existing or planned PRV instruments based on the design: CARMENES,[20] ESPRESSO,[21] EXPRES,[22] G-CLEF,[23] HARPS,[24] HARPS-N,[25] HPF,[26] MAROON-X,[27] NEID,[28] and PARAS.[29]

The baseline KPF spectrometer design is shown in Figure 7, with a summary of various parameters provided in Table 1. Light enters the core spectrometer following the fiber image reformatter, at the focal point of the primary collimator mirror (traditionally this would be the location of the spectrometer slit). The f/8 beam diverges past this point and then strikes the primary collimator mirror (an off-axis paraboloid). Upon reflection, the now collimated 200 mm diameter light beam travels to the echelle grating, located one primary collimator focal length away from the primary collimator. After diffraction by the echelle, the diverging monochromatic beams reflect from the primary collimator a second time. Because the echelle grating is rotated slightly out of

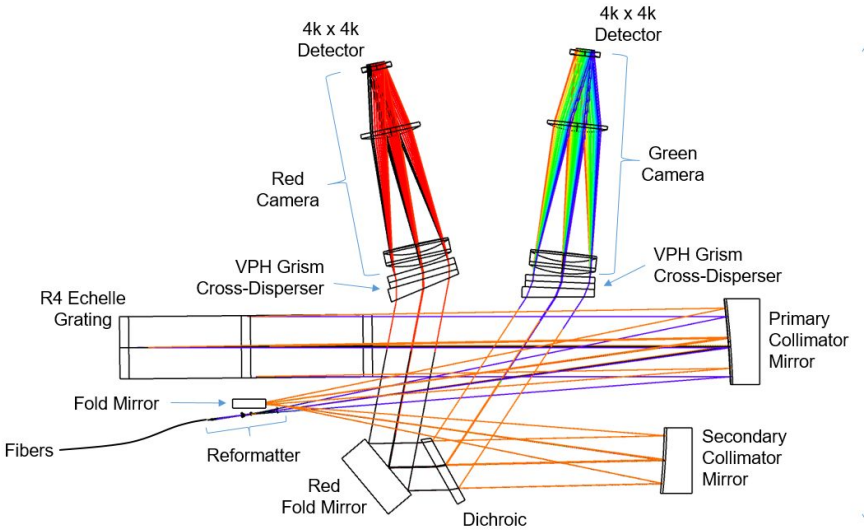

Figure 7. Optical layout of the KPF spectrometer.

Table 1. KPF spectrometer parameters summary table.

Parameter	**Value**
Optical design family	Asymmetric white pupil
Collimated beam diameter	200 mm
Collimator f/number	f/8
Asymmetric ratio	0.8
Resolving power	$>80{,}000$
Resolution element sampling	3 to 4 pixels (echelle dispersion direction)
Source fiber details	Science: 225 μm octagonal Sky: 225 μm octagonal, masked to 64 μm wide Simultaneous calibration: 100 μm octagonal, masked to 64 μm wide
Primary Collimator	Off-axis paraboloid 1600 mm focal length, f/8 beam Substrate: 452 mm tall x 284 mm wide (112 mm thick) Decenter: 240.5 mm
Primary disperser	R4 ($\theta_B = 75.96°$) echelle mosaic Master: Richardson MR263 31.6 grooves per mm Substrate: 840 mm x 214 mm x 125 mm
Secondary Collimator	Off-axis paraboloid 1280 mm focal length, f/8 beam Substrate: 430 mm tall x 217 mm wide (100 mm thick) Decenter: 153.5 mm
Dichroic	Transition wavelength: 590 nm Substrate: 415 mm tall x 246 mm wide (34 mm thick)
Wavelength coverage	Green channel: 445 nm to 600 nm Red channel: 598 nm to 870 nm
Cross-dispersers	VPH grisms Green VPH: 810 lines per mm Red VPH: 450 lines per mm
Green Camera	Focal Length: 495 mm, f/2.9 Largest aperture: 230 mm diameter
Red Camera	Focal Length: 495 mm, f/2.9 Largest aperture: 230 mm diameter
Detectors (Green and Red)	4k x 4k, 15 μm pixels

plane (the echelle gamma angle), the dispersed light does not return along the same path, and the pre- and post-diffraction beams are separated. Therefore, after reflecting from the collimator the second time, the dispersed light does not return to the entrance slit, but forms an intermediate focus to the side of the echelle. Just before the intermediate focus, a flat mirror is employed to fold the beam, to make the spectrometer footprint more compact.

After the fold mirror reflection, the light rays go through the intermediate focus, and then the diverging monochromatic beams are collimated by the secondary collimator mirror (an off-axis paraboloid). The monochromatic beam diameter here is 160 mm, owing to the secondary collimator having a focal length 0.8× that of the primary collimator (determined via a trade study in the conceptual design phase[6]). The converging

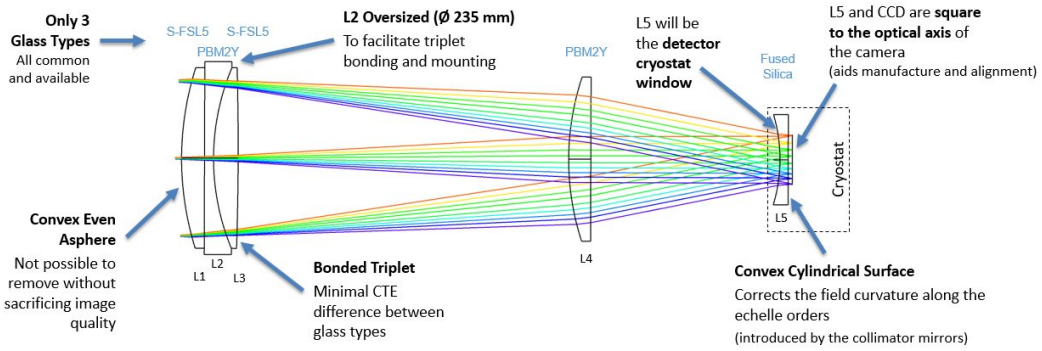

Figure 8. The green channel camera design, with design highlights indicated. This meridional view is in the cross-dispersion direction, with the blaze wavelengths of five echelle orders shown. The red channel design is very similar (the only differences being surface curvatures, spacings and aspheric coefficients).

monochromatic beams next encounter a dichroic beamsplitter, which reflects the green bandpass and transmits the red. The dichroic transition region start (demarcated by the 95% throughput point) was set just redward of the sodium doublet at 590 nm, to ensure these lines do not fall within the reduced throughput region of the dichroic crossover region.

After reflection, the green channel monochromatic beams continue to converge towards the white pupil, with the cross-dispersion grism (grating prism) located just beyond that point. This disperser consists of a shallow apex angle prism bonded to a volume phase holographic (VPH) grating. Following the grism, the light enters the camera, which then focuses the spectrum onto the CCD detector. The red channel monochromatic beams are transmitted through the dichroic, and are reflected by the red fold mirror (to steer the beam back on to the footprint of the optical bench), after which they also travel through a cross-dispersing grism and camera.

Both the green and red cameras are five-element Petzval designs (Figure 8), consisting of a bonded triplet, followed by a singlet lens, and finally a field flattener lens just before the CCD detector. Both the green and red cameras use the same glass types. The first surface of the triplet is a convex even asphere, and the final surface of the field flattener is a convex cylinder. The elements in both cameras are the same size, which allows for many common opto-mechanical assemblies between the two channels.

Winlight Systems has performed two detailed studies on the KPF cameras, during which the camera designs were optimized and also assessed for ghosting, schedule and technical risk, and manufacturability. Their conclusion was that neither camera presents significant risk. As part of the studies they also designed a passively athermalized camera barrel. They found the camera performance to be remarkably stable to laboratory-level bulk temperature changes over 20°C ± 2.5°C, using a camera barrel made up of sections of aluminum, stainless steel, and invar. This implies exceptional stability within our operating temperature range of 20°C ± 0.01°C, and we will explore this design further in the next project phase.

Since the 2016 SPIE paper,[6] updates with respect to the spectrometer design include:

- **Off-axis angle:** The off-axis angle of the primary collimator was increased from 7.5° to 8°. This change increased the beam clearances around the dichroic, echelle, reformatter and intermediate fold, and also made more room for the mechanical mounts of these optics.
- **Echelle:** The KPF echelle (a mosaic with two sub-gratings on a monolithic substrate) has been completed by Richardson Gratings.
- **Dichroic:** There will be a 0.5° wedge between the front and rear plano surfaces to suppress fringing from internal etalon effects that can form in plane-parallel plates. The dichroic thickness has also increased from 30 mm to 34 mm after discussions with vendors that a thicker substrate would better counteract stresses imparted by the coatings.

- **Grisms:** The grisms are now yawed at a 4.8° angle to the optical axis of the cameras, to steer a Fresnel ghost path off the detector (between the CCD and the VPH rear surface). The VPH gratings are now square in outline (vendor preference over circular gratings).

3.7 Detectors

The KPF detectors will be 4k x 4k CCDs, with 15 μm pixels. For both channels, we have chosen STA4850 devices from Semiconductor Technology Associates (STA). This is a new CCD based closely on the existing STA4150, and is expected to have the same performance as the STA4150.

A 30 μm-thick version of the STA4850 with a blue-sensitive "DESI" coating provides the best option for the KPF green arm. For the red arm (where fringing is more of a concern), a 100 μm-thick version with the red-tuned "LSST" coating was chosen. The simplification of using the same CCD architecture and package for both arms means that the same CCD electronics and cryostat detector mounts can be used in both channels, saving cost, complexity, time, and risk. Furthermore, the STA4850 CCDs are mounted in a package designed specifically for good thermal and mechanical stability.

The detector cryostats are being designed at SSL. UCO will be responsible for mounting the CCDs within the cryostats, and also the design of the detector electronics. UCO and Caltech will both be involved with testing the characterizing the entire system (consisting of CCD, electronics, and controllers). Both channels will utilize STA Archon CCD controllers.

3.8 Spectral Formats

Figure 9 shows the spectral formats of the green and red channels, as well as Zemax-generated[30] synthetic spectra. During the preliminary design phase the orders and wavelengths on each CCD were slightly adjusted, so that the sodium doublet is now placed one order inwards from the red edge of the green CCD. In addition, the start of the dichroic transition region was tied to a point just redward of the sodium doublet, ensuring that the throughput of these lines is not affected by the dichroic crossover. These choices then anchored the spectrum between the two channels, setting the orders and wavelengths on each CCD. This bandpass adjustment also brought the Ca IR triplet lines onto the red end of the red CCD (these are astrophysically important lines that can be utilized as stellar activity indicators).

Care was taken to square the orders and the resolution elements to the CCD rows and columns (on average). Squaring the orders to the CCD (by rotating the CCD) helps simplify the extraction of spectra in the data reduction pipeline, and squaring the resolution elements with the CCD (by rotating the slit, or in the KPF case the entire reformatter) avoids the resolution-smearing effects of line tilt. As such, the green CCD is clocked 2.43°, the red CCD is clocked 1.90°, and the reformatter is clocked 1.89°.

3.9 Calibration System

The KPF calibration system will reside in the observatory basement hallway near the spectrometer. This system will include the typical spectrometer calibration sources (Thorium-Argon lamps for wavelength calibration and a continuum source for flat-fielding), as well as a Fabry-Pérot etalon to provide a high line density source to track the instrument drifts. A separate broadband source will also feed a fiber to illuminate a diffuse source within the reformatter, for flat-fielding the entire CCD as opposed to flat fielding with the primary fibers, which only provides illumination within the orderlets (with undersampled edge pixels) and not between them.

As shown in Figure 2, two calibration fibers will travel up to the telescope, where the FIU will focus the calibration light onto the science and sky fibers (for calibrations between science exposures). A third calibration fiber will travel directly to the spectrometer, to provide a simultaneous calibration source during a science exposure.

The KPF calibration unit will consist of various off-the-shelf components (lenses, filters, beamsplitters and fiber holders) located on a standard optical breadboard. To switch between sources, we have adopted the system developed by the CARMENES team, where the lamps and sources are radially located on the faces of an octagon mount.[20] An advantage of this design is that both the sources and the fibers remain stationary during source

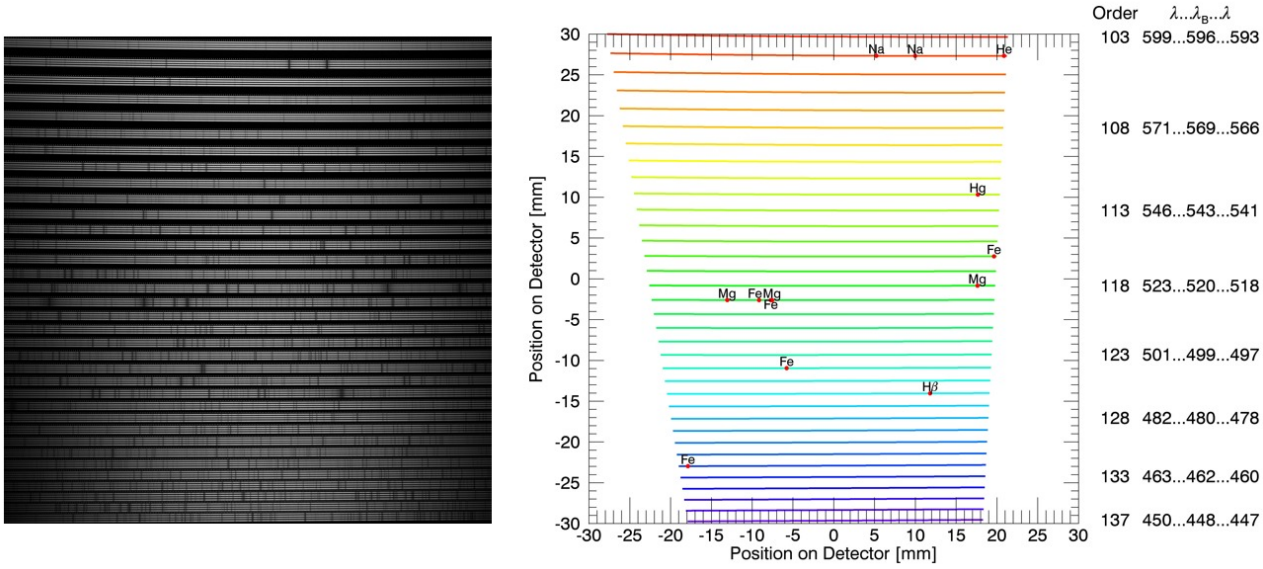

(a) Green Channel

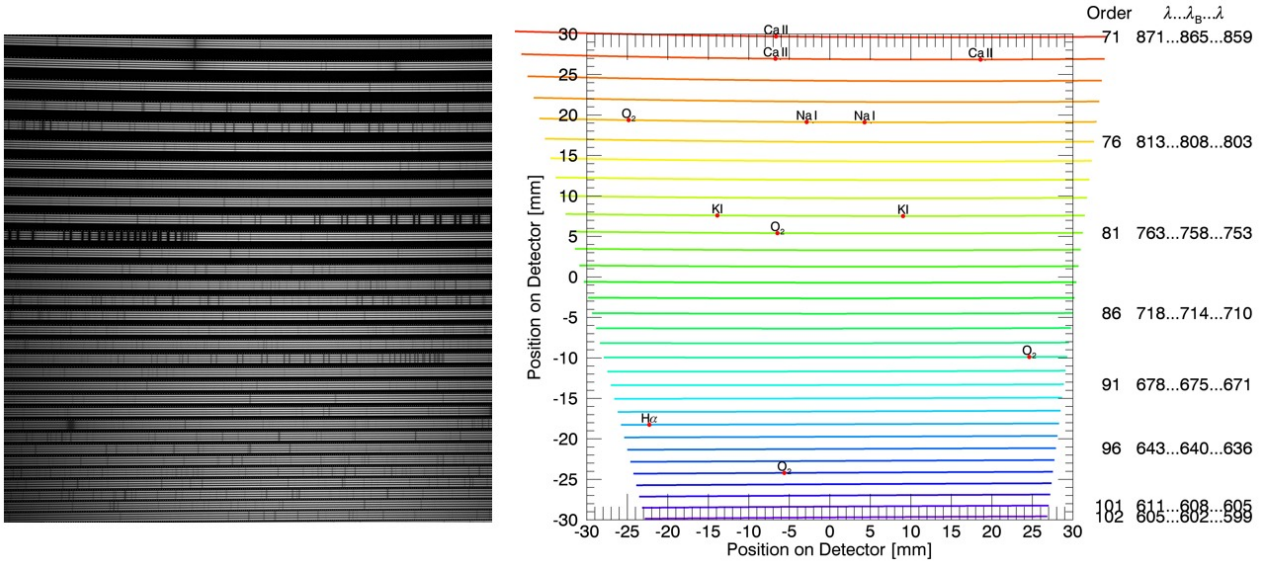

(b) Red Channel

Figure 9. Left: Zemax-generated synthetic KPF spectra for both channels. A solar spectrum was used for the three science slices and the sky fiber, and a Fabry-Pérot etalon source was used for the simultaneous calibration fiber. The echelle blaze efficiency profile was included within the Zemax model. Right: Echellograms showing the orders for each channel out to one free spectral range, with Fraunhofer and other absorption lines of interest indicated.

changes. To further select between various combinations of sources and fibers sending light to the spectrometer, several shutters are located throughout the system.

KPF will use a laser-locked Fabry Pérot etalon, built at Macquarie University, as the primary wavelength calibrator.[31–33] We selected this system for its long-term stability, excellent precision and low maintenance. The calibrator uses a Fabry-Pérot etalon with Zerodur spacer, which is thermally stabilized in a vacuum chamber.[34] Fed with a white light source, the etalon produces a highly uniform comb of unresolved lines spanning the whole wavelength range of the spectrometer, with a spacing of three resolution elements at the bluest wavelengths. The wavelength of a single etalon peak is continuously monitored by comparing it to the hyperfine transitions of the Rubidium D2 line at 780 nm using saturated absorption laser spectroscopy. We expect the long-term precision of the system to be better than $3\,\mathrm{cm\,s^{-1}}$.

3.10 Calcium H & K Spectrometer

A separate small spectrometer will be used to monitor the Calcium H & K lines as indicators of stellar activity that could mimic Doppler shifts. A consequence is that the main spectrometer does not need to cover an increased bandpass blueward to 385 nm, resulting in several important advantages: smaller optical coating bandpasses and hence higher efficiencies; less complicated camera designs; and also smaller detectors.

The science-based requirements for this instrument include: a bandpass of 385–405 nm (to include the lines themselves and adjacent areas of the continuum); a resolving power of $R = 8{,}000$; and a throughput equivalent to the main spectrometer (to ensure that Calcium H & K exposures do not take longer than the main spectrometer).

Initially several simple designs were considered, however, given the resolving power requirement coupled with the AΩ of the Keck telescope, such an approach leads to either a large collimated beam diameter (and hence large optics and grating), or an impractically narrow slit. (For the same reasons a search for an off-the-shelf spectrometer yielded no viable options). To meet the resolving power requirement within an instrument of a reasonable size, an R4 echelle grating was chosen as the primary dispersing element. With this approach, available resolving power was traded for a smaller instrument (with a collimated beam diameter of 50 mm) and a wider slit (for increased throughput).

The preliminary optical design for this spectrometer is shown in Figure 10. The double-pass design[35–38] was chosen for this instrument, owing to its smaller size and lower part count than an equivalent white pupil spectrometer. Glasses from the DESI blue camera[39] design were used for the camera/collimator. The design of this instrument will be further refined in the next project phase.

3.11 Exposure Meter

An exposure meter will be employed to determine the chromatic photon-weighted mid-exposure time of each observation, required to accurately determine the barycentric correction and account for the movement of the Earth during an observation.

During the preliminary design phase this instrument changed from a simple photomultiplier-based device to a low-resolution ($R = 100$) spectrometer covering the main spectrometer bandpass. This change allows the exposure mid-time calculation to account for chromatic effects including differential atmospheric refraction, differential atmospheric attenuation with airmass, and the chromatic performance of the guide system. The barycentric correction(s) can then be computed for multiple distinct wavebands spanning the spectrometer's bandpass.[40,41]

Commercial, off-the-shelf mini-spectrometers were initially considered but had several undesirable characteristics: high thermal noise; datafile output (not raw images); and no control over calibration. As a result, it was determined that designing a custom spectrometer system was the best option.

Analysis showed that the exposure meter could make the required measurement if it received 1% of the flux that the main spectrometer receives. This was achievable by collecting the light from the two otherwise-unused outboard slices on the fiber face, as shown in Figure 10. The preliminary optical design consists of a custom doublet collimator lens, a Thorlabs prism, a Navitar camera lens, and an off-the-shelf detector like the SBIG STT-3200 shown in the figure.

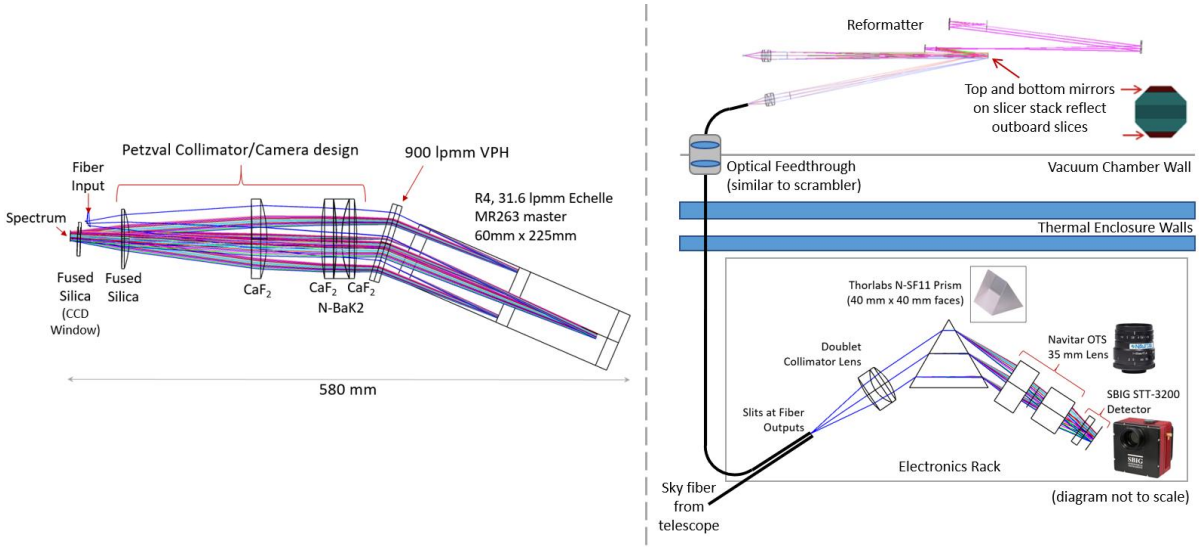

Figure 10. Left: Optical layout of the KPF Calcium H & K spectrometer. The larger camera lenses are 80 mm in diameter. Right: The KPF exposure meter system. The system collects light from the otherwise unused outboard slices on the science fiber. This light is then fed into an optical fiber which travels outside of the spectrometer thermal enclosure to the exposure meter itself. Within the optical layout the camera model is shown in the Zemax "black box" format (as obtained from the manufacturer), which allows for accurate ray-tracing but hides the proprietary lens details from the user.

4. OPTO-MECHANICAL DESIGN

In order to measure sub-m s^{-1} Doppler shifts, it is critical for a PRV spectrometer to have high mechanical and environmental stability. This section will outline the KPF opto-mechanical design.

4.1 Optical Bench and Optical Mounts

Stability analyses undertaken within Zemax have demonstrated that nanometer-level movements of the KPF optics cause spectral shifts at the m s^{-1} level.[42] Within PRV spectrometers such movements are typically constrained by exquisite milli-Kelvin or better temperature control to minimize expansion and contraction effects (for example, HARPS[24] and HPF[43]). The KPF design intends to minimize the effect of temperature changes or gradients by utilizing low coefficient of thermal expansion (CTE) materials throughout the spectrometer. Minimizing local optic movements that shift the beam vertically with respect to the table is especially critical, as this is along the direction of echelle dispersion within the KPF design.

A unique aspect of KPF is the use of a Zerodur optical bench to support the spectrometer, as shown in Figure 11. Our bench source is a 2 m diameter by 0.4 m thick disk of Zerodur that was purchased for, (but then not utilized by), a previous SSL project (Figure 12, left). The primary advantage of a Zerodur bench is its small CTE value, and our particular disk has an extremely low CTE value (approximately 0.000 $\pm$ 0.004 x 10^{-6} K^{-1}, as measured by Schott). This CTE value is orders of magnitude smaller than metals typically used in optical benches.

We intend to take full advantage of the low CTE bench by mechanically contacting optics and mounts - also made of Zerodur, where possible - to the Zerodur bench. We are specifically avoiding high CTE materials which are commonly used to mount optics (i.e. metals, RTV, plastics and epoxies). As such, we expect the KPF spectrometer to have a very high level of mechanical and thermal stability.

The full Zerodur disk must be modified as it weighs 3177 kg and will not fit through the access hatch into the observatory basement. Therefore, we intend to cut the disk as shown in the right side of Figure 12. Also shown in the figure is our plan to utilize portions of the disk as the source for optical substrates.

Our preliminary mount design will utilize pockets CNC-machined into the top surface of the optical bench, as shown on the left side of Figure 13. Each optic will sit within one of these pockets, with three vertical and three

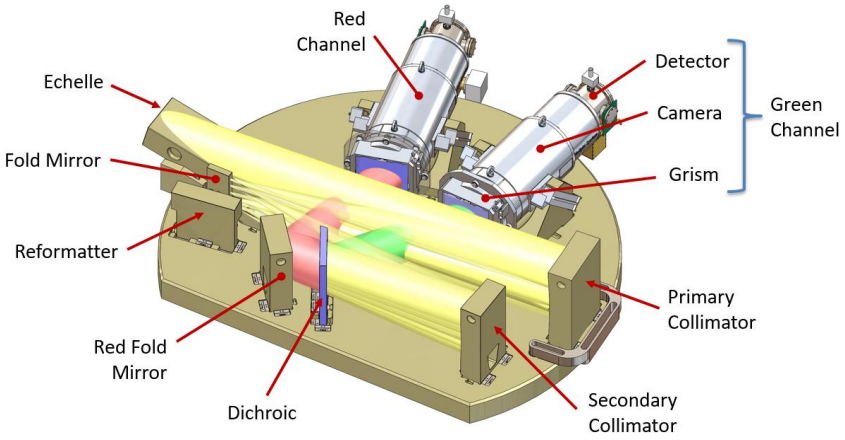

Figure 11. The KPF opto-mechanical design, with the optical elements supported by a Zerodur bench.

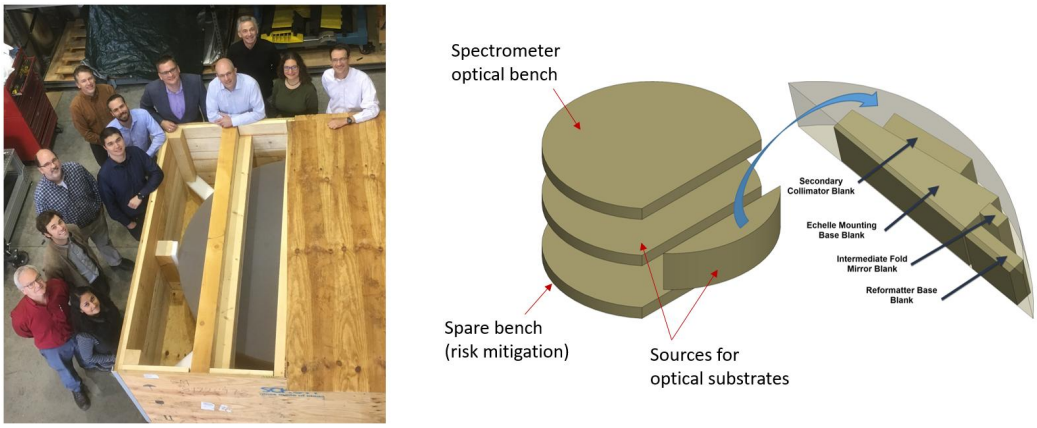

Figure 12. Left: KPF team members and the Zerodur disk (partially uncovered within its shipping crate). Right: Planned modifications to the Zerodur disk.

horizontal shim stacks used between the optic and the pocket walls (as shown in the right side of Figure 13). The optic will then be held in this location by spring force. With this method, there is only Zerodur between the optic (or mount) and the Zerodur bench, and the expansion and contraction of the springs cannot influence the position of the optic (rather only slightly affect the spring force they apply to the optic). Three springs are required for each optic: one vertical spring (to provide downward force against the pocket floor), and two horizontal springs (to provide sideways force against the pocket reference walls).

For a more in-depth description of the KPF opto-mechanical design, the reader is directed to Smith et al. (2018)[44] within these proceedings.

4.2 Vacuum Chamber, Optical Bench Support, and Installation Details

In order to isolate the spectrometer from its environment, it will be placed within a vacuum chamber (for isolation against convective thermal disturbances and changes in atmospheric pressure), and also within an insulated room in the observatory basement (for isolation against temperature changes).

The current KPF vacuum chamber design is shown at the left of Figure 14. Two hinged doors allow access to the interior. To minimize the fiber length to the telescope, the two scrambler systems are located on the door closest to the coudé tunnel. Within the chamber, the optical bench will be supported on five vacuum-compatible Minus K CM-1 isolators, to prevent vibrations or chamber deflections from influencing the positions of optics on the bench. These isolators will be supported on a platform, which in turn is supported by three legs that directly attach to the chamber itself.

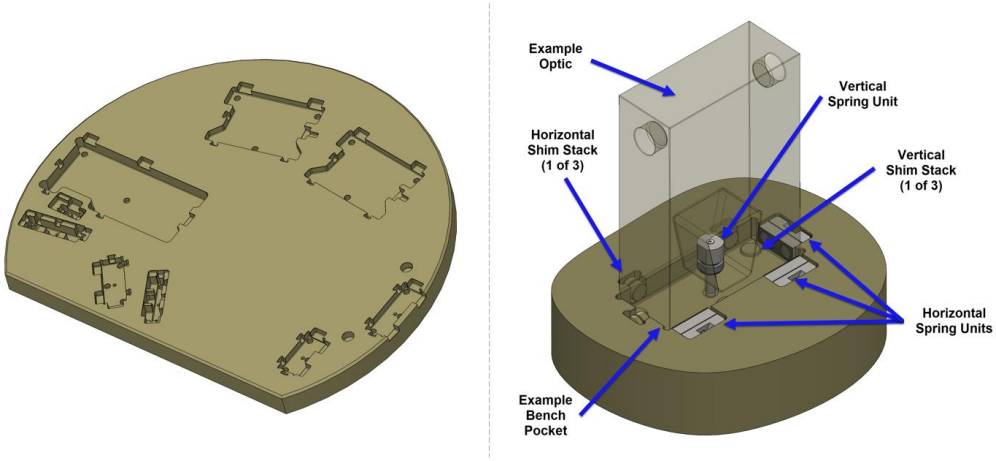

Figure 13. Left: Pockets will be CNC-milled into the top of the Zerodur bench to locate the spectrometer optics. Right: Zerodur shims will be used to register the optics against the bench, with springs applying force to maintain the Zerodur-to-Zerodur contact.

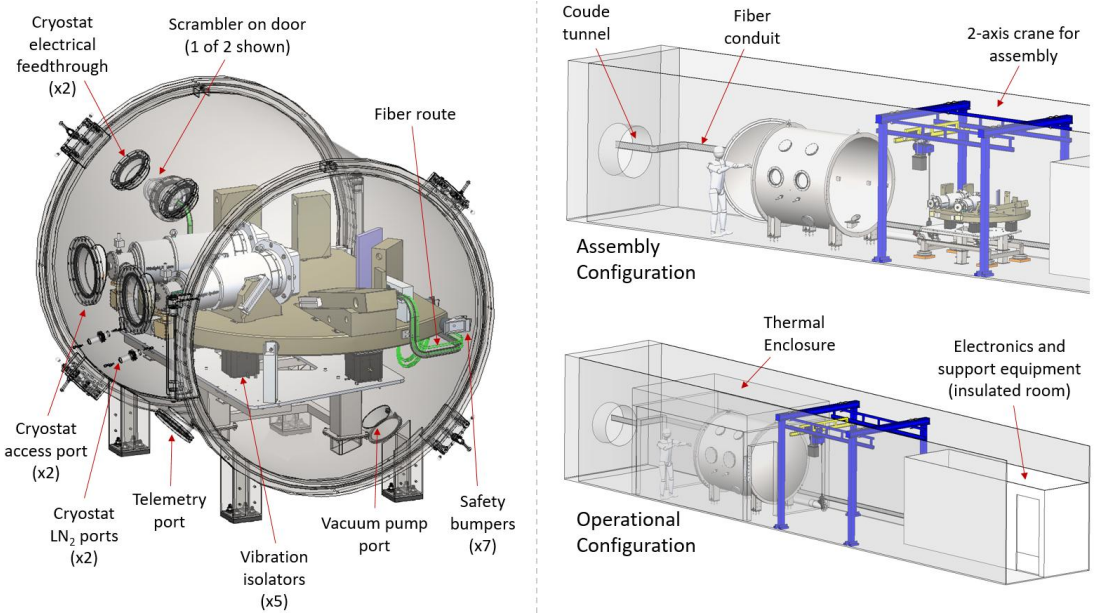

Figure 14. Left: The KPF vacuum chamber. The chamber is 1960 mm in diameter and 2600 mm long. The safety bumpers constrain excessive bench movement but are not in constant contact with the bench. Right: Layout of the spectrometer and its support equipment in the observatory basement hallway (for both assembly and operational configurations).

Prior to shipment, the optics will be removed from the bench. At the observatory, the optics will be re-installed using a 2-axis bridge crane, with the bench sitting on the isolators and support platform. The bench and support assembly will then be rolled into the vacuum chamber using a custom cart and track system. Details of the basement layout for the assembly and operational configurations are shown in Figure 14.

5. DATA REDUCTION PIPELINE

Groundbreaking and believable exoplanet discovery relies heavily on the precision and accuracy of the reduction pipelines through which data is processed. Cross-dispersed echelle spectra are inherently complex datasets; in addition, next generation spectrometers will require long-baseline calibration and subtle corrections based on a thorough knowledge of the instrument, making it very challenging for external users to properly reduce and analyze this data in the context of environmental and observational factors. Thus, KPF will be delivered together

with a sophisticated and fully automated Data Reduction Pipeline (DRP) created by the instrument team. The KPF DRP draws on extensive heritage from the PARAS DRP,[29,45] which has demonstrated precision at the $\leq$ 1 m s^{-1} level. Our team is also descended from the pioneers of the iodine-cell calibration technique for precision RV measurements, with a decades-long legacy in the creation, implementation, and evolution of the Keck HIRES pipeline and RV science analysis tools.

Using modern software engineering practices like rigorous version control, modular development, and in-built unit/regression testing, the KPF DRP will be fully integrated with the Keck Observatory Archive (KOA). Drawing on the NEID pipeline architecture, the KPF DRP will deliver three levels of data products broadly categorized as Level 0 (raw), Level 1 (processed), and Level 2 (high-level derived). Of most relevance to the majority of users, derived data products will include cross-correlation functions, stellar activity metrics, telluric correction parameters, and final RV measurements for each observation. The pipeline will be strongly coupled to a strict calibration routine for the instrument, executed every night that the telescope is available, such that every single observation can be tied back to the entire history of the KPF system. As such, we recognize the DRP as an essential project subsystem that is critical to the achievement of our primary science goals, as well as a foundational tool for future developments in the field.

6. PERFORMANCE METRICS

Within this final section, three tools are presented that are utilized to track instrument performance during the design process: the Doppler error budget; a photon noise simulator; and a model to estimate throughput.

6.1 Doppler Error Budget

Any instrumental perturbation that produces a bulk displacement, warping, or PSF variation of the echelle spectrum on the CCD in the spectral dispersion direction is indistinguishable from an astrophysical Doppler shift. This section briefly summarizes our efforts to quantify the possible sources of false Doppler shifts due

KPF PDR error budget spreadsheet, all units in cm/s

Instrumental errors (uncalibratable)	22.23
Fiber & illumination	18.47
Calibration source modal noise	2.50
Continuum modal noise	2.50
Near-field scrambling	8.00
Far-field scrambling	5.00
Stray light & ghosts	5.00
Fiber-fiber contamination	5.00
Polarization	2.00
Focal ratio degradation (science)	7.80
Focal radio degradation (calibration)	7.80
Double scrambler drift	8.00
Detector effects	7.07
Pixel center offsets	5.00
Charge transfer inefficiency	5.00
Barycentric correction	1.73
Algorithms	1.00
Exposure midpoint time	1.00
Coordinates and proper motion	1.00
Reduction pipeline	10.00
Software algorithms	10.00

Instrumental errors (calibratable)	18.53
Calibratable error contribution	1.85
Thermo-mechanical	12.13
Thermal stability (grating)	3.00
Thermal stability (cross-disp.)	5.00
Thermal stability (bench)	4.00
Thermal stability (cameras)	6.80
Vibrational stability	1.00
Pressure stability	5.00
Zerodur phase change (Echelle)	5.00
Detector effects	14.00
Pixel inhomogeneities	5.00
CCD thermal expansion	5.00
Readout thermal change	11.00
Charge transfer inefficiency	5.00

Calibration source (uncalibratable)	15.00
Calibration accuracy	11.18
Wavelength stability	10.00
Photon noise	5.00
Calibration process	10.00
Software algorithms	10.00
External errors (uncalibratable)	18.94
Telescope	12.60
Guiding (")	0.05
ADC	5.80
Focus	5.00
Injection angle variations	10.00
Atmospheric effects	14.14
Micro-telluric contamination	10.00
Scattered sunlight contamination	10.00
Total instrumental error (cm/s):	32.8824

Figure 15. Our full KPF error budget table showing individual error contributions from noise sources. Major subsystems are broken out in sub-fields with individual contributions to the total error budget listed next to the system labels. All terms are separated using calibratable and uncalibratable tags. Calibratable errors are tracked by the calibration source, while uncalibratable terms are not. Color codes for each term indicate level of detail in constraining particular error contributions, with well understood (green), moderately constrained (yellow), and more poorly constrained (red) terms listed. The final, single-point measurement precision is derived by combining uncalibratable and calibratable errors in quadrature. We conservatively assume 10% of the calibratable errors are left uncorrected. For detailed descriptions of individual error terms, see Halverson et al. (2016).[46]

to instrumental perturbations. We include error sources from the KPF spectrometer, wavelength calibration process, telescope and guiding system, and the Earth's atmosphere. We follow the systems engineering approach adopted by Podgorski et al. (2014)[47] and Halverson et al. (2016)[46] for the G-CLEF and NEID instruments, respectively, to construct a comprehensive, single-point measurement error budget for the full KPF system, as shown in Figure 15. Following Halverson et al. (2016), we distinguish between calibratable (tracked by the KPF calibration fiber) and non-calibratable (not tracked by wavelength calibrator) errors when grouping and combining individual error terms. The interleaved orders of the calibration spectrum ideally experience the same displacement as the stellar orders. Thus, by precisely measuring and tracking displacements of the calibration spectrum, the wavelength solution for the stellar spectrum can precisely track these displacements with high accuracy. Effectively, calibratable Doppler errors can be subtracted off to a significant degree because the science spectrum experiences almost the same displacements as the calibration spectrum.

6.2 Photon Noise Simulations

Calculating the photon-limited velocity measurement precision is essential for estimating the expected on-sky performance of KPF. Here we briefly summarize the calculations performed to estimate the Doppler RV measurement uncertainty due to stellar photon noise. Following the methodology described in Bouchy et al. (2001)[48] and Murphy et al. (2007),[49] we estimate the expected photon-noise limit for the KPF instrument by scaling synthetic stellar spectra using modeled atmospheric and instrumental efficiency curves (see Section 6.3). We also include expected read-noise from our two 4k × 4k CCDs, as this will add additional noise to recorded spectra. Results from our calculations are shown in Figure 16 for an example target, highlighting how KPF's broad wavelength coverage will enable high precision (< 1 m s^{-1}) RV monitoring of a wide variety of different stars. Finally, Figure 17 shows the limiting magnitudes KPF can reach for a desired total measurement precision, emphasizing how KPF is uniquely suited to observe targets that are too faint for classical RV surveys on smaller telescopes (V>12).

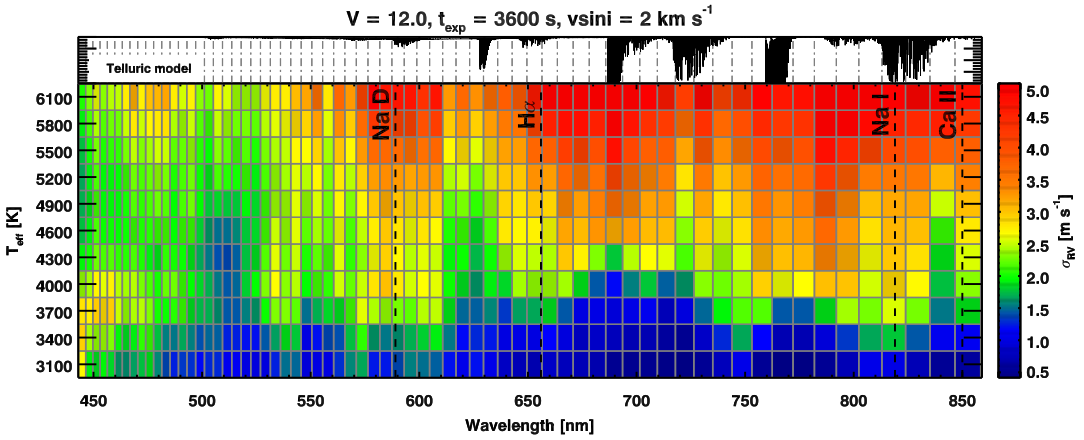

Figure 16. Relative Doppler information content comparison between spectral types as a function of wavelength for the KPF green and red channels. Individual color bins are separated for each echelle diffraction order, and the colors trace the relative amount of Doppler information content in each bin. Over-plotted are the wavelengths of relevant stellar activity indicators that are captured in the KPF bandpass. Each grid point represents a separate echelle order. Also shown is a telluric model for Mauna Kea at z = 30 degrees. The wide bandwidth will allow KPF to reach high precision on a variety of different stars, from cool M-dwarfs to Sun-like stars.

6.3 Throughput Estimate

Figure 18 shows the results of the KPF efficiency model, including surfaces from the top of the telescope to the spectrometer CCDs, and including all three science slices. Both channels have peak efficiencies of 8.2%. A conservative approach was taken when constructing this model, by including measurements of coatings fabricated for other projects, or by using worst-case "production minimum" efficiencies provided by vendors.

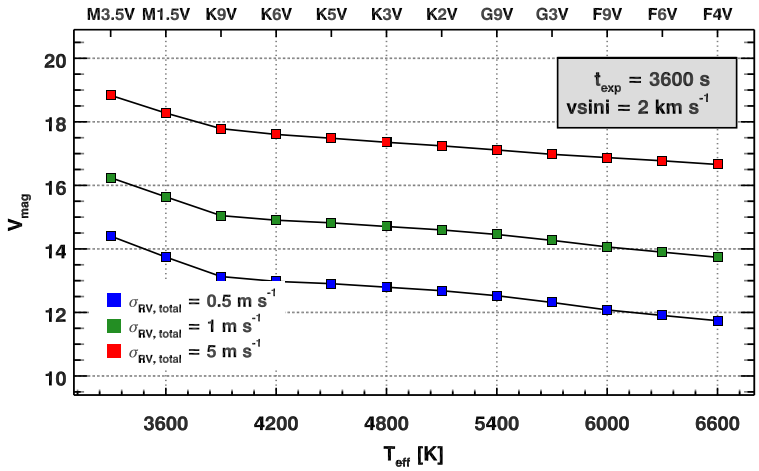

Figure 17. Estimated limiting magnitudes to reach a fixed single-point velocity uncertainty limit, $\sigma_{\rm total} = \sqrt{\sigma^2_{\rm inst} + \sigma^2_{\rm phot}}$, as a function of stellar temperature ($T_{\rm eff}$) and brightness ($V_{\rm mag}$). Brightness limits are for a total Doppler uncertainty of 0.5 m s^{-1} (blue), 1.0 m s^{-1} (green), and 5.0 m s^{-1} (red) for a 1 hr exposure. Sources of stellar jitter are not accounted for. The assumed instrumental error, $\sigma_{\rm inst}$, is 0.35 m s^{-1}.

The dichroic crossover region causes the "dip" between channels at approximately 600 nm. The redmost order on the green channel (order 103) also appears as a partial order on the red channel. The overall shape of each channel is driven by the efficiency envelopes of the VPH gratings. In addition, the blue side of the green channel is further affected by the preferential blue attenuation of the optical fibers. The red side of the red channel is also affected by the aluminum coatings on the Keck telescope primary, secondary, and tertiary mirrors.

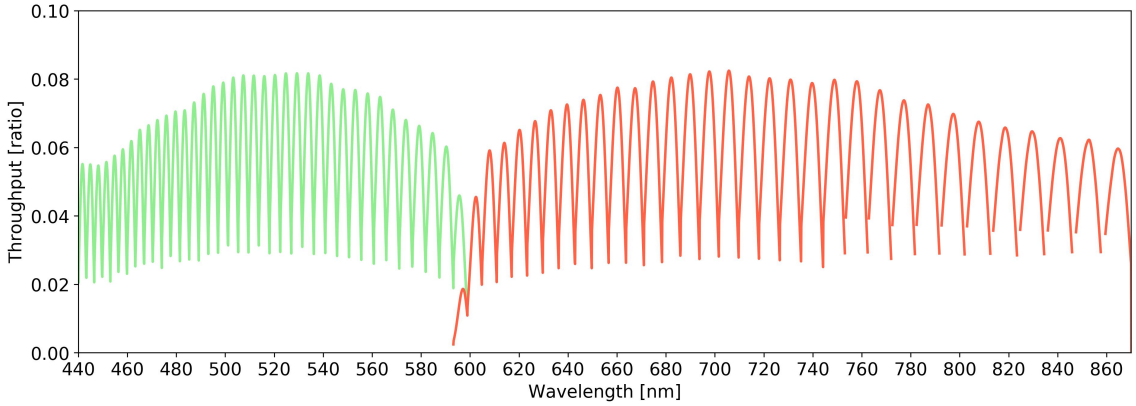

Figure 18. The KPF predicted throughput across the entire instrument bandpass, from the top of the telescope to the spectrometer CCD, for the green and red channels (colored appropriately). Efficiency profiles across echelle orders are shown out to one free spectral range or to the edge of the detector (whichever occurs first). The median seeing value of 0.7 arcseconds FWHM was used for this calculation.

ACKNOWLEDGMENTS

The authors thank the Heising-Simons Foundation, the W.M. Keck Foundation, the University of California, Berkeley, the California Institute of Technology, and the University of Hawaii for financial support of KPF. The authors also wish to thank Winlight Systems for their valuable contributions to the designs of the reformatter and cameras, as well as the DESI project for sharing their camera designs and their expertise with optical fibers. This work was performed by SPH under contract with the Jet Propulsion Laboratory (JPL) funded by NASA through the Sagan Fellowship Program executed by the NASA Exoplanet Science Institute.

REFERENCES

[1] Howard, A. W. et al., "The Occurrence and Mass Distribution of Close-in Super-Earths, Neptunes, and Jupiters," *Science* **330**, 653 (Oct. 2010).

[2] Mayor, M. et al., "The HARPS search for southern extra-solar planets XXXIV. Occurrence, mass distribution and orbital properties of super-Earths and Neptune-mass planets," *arXiv:1109.2497* (Sept. 2011).

[3] Petigura, E. A. et al., "Prevalence of Earth-size planets orbiting Sun-like stars," *Proceedings of the National Academy of Science* **110**, 19273–19278 (Nov. 2013).

[4] Howard, A. W. et al., "Planet Occurrence within 0.25 AU of Solar-type Stars from Kepler," *ApJ* **201**, 15 (Aug. 2012).

[5] Sullivan, P. W. et al., "The Transiting Exoplanet Survey Satellite: Simulations of Planet Detections and Astrophysical False Positives," *ApJ* **809**, 77 (Aug. 2015).

[6] Gibson, S. R. et al., "KPF: Keck Planet Finder," in [*Ground-based and Airborne Instrumentation for Astronomy VI*], *Proc. SPIE* **9908**, 990870 (Aug. 2016).

[7] Prochaska, J. X. et al., "Keck 1 deployable tertiary mirror (K1DM3)," in [*Ground-based and Airborne Telescopes IV*], *Proc. SPIE* **8444**, 84444R (Sept. 2012).

[8] Queloz, D. et al., "The Fiber-Fed Spectrograph, a Tool to Detect Planets," in [*IAU Colloq. 170: Precise Stellar Radial Velocities*], *Astronomical Society of the Pacific Conference Series* **185**, 13 (1999).

[9] Perruchot, S. et al., "Higher-precision radial velocity measurements with the SOPHIE spectrograph using octagonal-section fibers," in [*SPIE Conference Series*], *SPIE Conference Series* **8151** (Sept. 2011).

[10] Avila, G., "FRD and scrambling properties of recent non-circular fibres," in [*Ground-based and Airborne Instrumentation for Astronomy IV*], *Proc. SPIE* **8446**, 84469L (Sept. 2012).

[11] Hunter, T. R. and Ramsey, L. W., "Scrambling properties of optical fibers and the performance of a double scrambler," *PASP* **104**, 1244–1251 (Dec. 1992).

[12] Avila, G. et al., "Performances of HARPS and FEROS fibers in La Silla ESO Observatory," in [*Ground-based Instrumentation for Astronomy*], *Proc. SPIE* **5492**, 669–676 (Sept. 2004).

[13] McCoy, K. S. et al., "Optical fiber modal noise in the 0.8 to 1.5 micron region and implications for near infrared precision radial velocity measurements," in [*Ground-based and Airborne Instrumentation for Astronomy IV*], *Proc. SPIE* **8446**, 84468J (Sept. 2012).

[14] Plavchan, P. P. et al., "Precision near-infrared radial velocity instrumentation II: noncircular core fiber scrambler," in [*Techniques and Instrumentation for Detection of Exoplanets VI*], *Proc. SPIE* **8864**, 88640G (Sept. 2013).

[15] Mahadevan, S. et al., "Suppression of Fiber Modal Noise Induced Radial Velocity Errors for Bright Emission-line Calibration Sources," *ApJ* **786**, 18 (May 2014).

[16] Roy, A. et al., "Scrambling and modal noise mitigation in the Habitable Zone Planet Finder fiber feed," in [*Ground-based and Airborne Instrumentation for Astronomy V*], *Proc. SPIE* **9147**, 91476B (July 2014).

[17] Sirk, M. M. et al., "An optical fiber double scrambler and mechanical agitator system for the Keck Planet Finder spectrograph," *Proc. SPIE* **10702** (Aug. 2018).

[18] Vivès, S. et al., "A set of Zemax user-defined surfaces to model slicer mirrors," *Proc. SPIE* **6273** (2006).

[19] Vivès, S. et al., "New technological developments in integral field spectroscopy," in [*Advanced Optical and Mechanical Technologies in Telescopes and Instrumentation*], *Proc. SPIE* **7018**, 70182N (July 2008).

[20] Quirrenbach, A. et al., "CARMENES instrument overview," in [*Ground-based and Airborne Instrumentation for Astronomy V*], *Proc. SPIE* **9147**, 91471F (July 2014).

[21] Spanò, P. et al., "Very high-resolution spectroscopy: the ESPRESSO optical design," in [*Ground-based and Airborne Instrumentation for Astronomy IV*], *Proc. SPIE* **8446**, 84467V (Sept. 2012).

[22] Jurgenson, C. et al., "EXPRES: a next generation RV spectrograph in the search for earth-like worlds," in [*Ground-based and Airborne Instrumentation for Astronomy VI*], *Proc. SPIE* **9908**, 99086T (Aug. 2016).

[23] Szentgyorgyi, A. et al., "The GMT-Consortium Large Earth Finder (G-CLEF): an optical Echelle spectrograph for the Giant Magellan Telescope (GMT)," in [*Ground-based and Airborne Instrumentation for Astronomy VI*], *Proc. SPIE* **9908**, 990822 (Aug. 2016).

[24] Mayor, M. et al., "Setting New Standards with HARPS," *The Messenger* **114**, 20–24 (Dec. 2003).

[25] Cosentino, R. et al., "Harps-N: the new planet hunter at TNG," *Proc. SPIE* **8446** (Sept. 2012).
[26] Mahadevan, S. et al., "The Habitable-zone Planet Finder: A status update on the development of a stabilized fiber-fed near-infrared spectrograph for the for the Hobby-Eberly telescope," in [*Ground-based and Airborne Instrumentation for Astronomy V*], *Proc. SPIE* **9147**, 91471G (July 2014).
[27] Seifahrt, A. et al., "Development and construction of MAROON-X," in [*Ground-based and Airborne Instrumentation for Astronomy VI*], *Proc. SPIE* **9908**, 990818 (Aug. 2016).
[28] Schwab, C. et al., "Design of NEID, an extreme precision Doppler spectrograph for WIYN," in [*Ground-based and Airborne Instrumentation for Astronomy VI*], *Proc. SPIE* **9908**, 99087H (Aug. 2016).
[29] Chakraborty, A. et al., "The PRL Stabilized High-Resolution Echelle Fiber-fed Spectrograph: Instrument Description and First Radial Velocity Results," *PASP* **126**, 133 (Feb. 2014).
[30] Gibson, S. R. and Wishnow, E. H., "A method for generating a synthetic spectrum within Zemax," in [*Systems Engineering V: Tools and Processes*], *Proc. SPIE* **9911** (June 2016).
[31] Schwab, C. et al., "Rubidium traced etalon wavelength calibrators: towards deployment at observatories," in [*Ground-based and Airborne Instrumentation for Astronomy VI*], *Proc. SPIE* **10702** (Aug. 2018).
[32] Schwab, C. et al., "Stabilizing a Fabry-Perot Etalon Peak to 3 cm s^{-1} for Spectrograph Calibration," *PASP* **127**, 880 (Sept. 2015).
[33] Stürmer, J. et al., "Rubidium-traced white-light etalon calibrator for radial velocity measurements at the cm s^{-1} level," *Journal of Astronomical Telescopes, Instruments, and Systems* **3**, 025003 (Apr. 2017).
[34] Wildi, F. et al., "A Fabry-Perot calibrator of the HARPS radial velocity spectrograph: performance report," in [*Ground-based and Airborne Instrumentation for Astronomy III*], *Proc. SPIE* **7735**, 77354X (July 2010).
[35] Libbrecht, K. G. and Peri, M. L., "A fiber-fed echelle spectrograph for the Hale 5-m telescope," *PASP* **107**, 62–67 (Jan. 1995).
[36] Bernstein, R. et al., "MIKE: A Double Echelle Spectrograph for the Magellan Telescopes at Las Campanas Observatory," in [*Instrument Design and Performance for Optical/Infrared Ground-based Telescopes*], *Proc. SPIE* **4841**, 1694–1704 (Mar. 2003).
[37] Crane, J. D. et al., "The Carnegie Planet Finder Spectrograph: integration and commissioning," in [*Ground-based and Airborne Instrumentation for Astronomy III*], *Proc. SPIE* **7735**, 773553 (July 2010).
[38] Vogt, S. S. et al., "APF - The Lick Observatory Automated Planet Finder," *PASP* **126**, 359 (Apr. 2014).
[39] Jelinsky, P. et al., "The BigBOSS spectrograph," in [*Ground-based and Airborne Instrumentation for Astronomy IV*], *Proc. SPIE* **8446**, 844668 (Sept. 2012).
[40] Landoni, M. et al., "ESPRESSO front end exposure meter: a chromatic approach to radial velocity correction," in [*Ground-based and Airborne Instrumentation for Astronomy V*], *Proc. SPIE* **9147** (Aug. 2014).
[41] Blackman et al., "Accounting for Chromatic Atmospheric Effects on Barycentric Corrections," *ApJ* **837**, 18 (Mar. 2017).
[42] Gibson, S. R., "Tolerancing a radial velocity spectrometer within Zemax," in [*Systems Engineering V: Tools and Processes*], *Proc. SPIE* **9911**, 991190 (June 2016).
[43] Stefánsson, G. K. et al., "Ultra-stable temperature and pressure control for the Habitable-zone Planet Finder spectrograph," in [*Ground-based and Airborne Instrumentation for Astronomy VI*], *Proc. SPIE* **9908** (2016).
[44] Smith, C. et al., "Keck Planet Finder: Zerodur optical bench mechanical design," in [*Ground-based and Airborne Instrumentation for Astronomy VI*], *Proc. SPIE* **10702** (Aug. 2018).
[45] Roy, A. et al., "Precision velocimetry planet hunting with PARAS: current performance and lessons to inform future extreme precision radial velocity instruments," in [*Ground-based and Airborne Instrumentation for Astronomy VI*], *Proc. SPIE* **9908**, 99086R (Aug. 2016).
[46] Halverson, S. et al., "A comprehensive radial velocity error budget for next generation Doppler spectrometers," *ArXiv e-prints* (July 2016).
[47] Podgorski, W. et al., "A novel systems engineering approach to the design of a precision radial velocity spectrograph: the GMT-Consortium Large Earth Finder (G-CLEF)," in [*Ground-based and Airborne Instrumentation for Astronomy V*], *SPIE Conference Series* **9147**, 91478W (July 2014).
[48] Bouchy, F. et al., "Fundamental photon noise limit to radial velocity measurements," *A&A* **374**, 733–739 (Aug. 2001).
[49] Murphy, M. T. et al., "High-precision wavelength calibration of astronomical spectrographs with laser frequency combs," *MNRAS* **380**, 839–847 (Sept. 2007).